Journal of ELECTRONIC MATERIALS, Vol. 50, No. 6, 2021
https://doi.org/10.1007/s11664-021-08856-1

ORIGINAL RESEARCH ARTICLE

Polyaniline/Graphitic Carbon Nitride Nanocomposites with Improved Thermoelectric Properties

VOLKAN UGRASKAN [1,2] and FERDANE KARAMAN[1,3]

1.—Department of Chemistry, Yildiz Technical University, 34220 Istanbul, Turkey. 2.—e-mail: ugraskan@yildiz.edu.tr. 3.—e-mail: ferdanekaraman@yahoo.com

In this study, we aimed to investigate the effects of graphitic carbon nitride (g-C_3N_4) on the thermoelectric (TE) properties of camphorsulfonic acid (CSA) doped polyaniline (PANI). For this purpose, g-C_3N_4 was synthesized at 550°C using guanidine hydrochloride as a precursor. Later, PANI was synthesized by oxidative chemical polymerization and doped with CSA. Finally, PANI-CSA/g-C_3N_4 composites were prepared by ultrasonic homogenization with different weight ratios of g-C_3N_4. The composites showed positive Seebeck coefficients which are the characteristics of *p-type* semiconductors. The Seebeck coefficient of PANI-CSA enhanced from 10 μV K^{-1} to 472 μV K^{-1} with the incorporation of g-C_3N_4. Furthermore, the power factor (PF) of the composites reached a maximum at 70.75 μW m^{-1} K^{-2} which is almost 500 times higher compared to pristine PANI-CSA. This indicates that g-C_3N_4 is a promising additive to be used in polymer-based TE materials that can be used around room temperature.

Key words: Polyaniline, graphitic carbon nitride, thermoelectric, composite

INTRODUCTION

Thermoelectric (TE) energy conversion is an important method that provides direct conversion of heat to electrical energy or vice versa. Applications of TE devices that are not only used in energy conversion include cooling modules of some devices such as optical materials, aviation applications, and telecommunications equipment.[1]

The energy conversion performance of the materials used in TE devices can be obtained by the dimensionless figure of merit $ZT = S^2\sigma T/\kappa$ where S, σ, T, and κ correspond to Seebeck coefficient, electrical conductivity, absolute temperature, and thermal conductivity, respectively.[2] Although the traditional inorganic semiconductor TE materials have high conductivity and Seebeck coefficient, their efficiencies decrease to less than 30% due to their high thermal conductivity, and also they have disadvantages such as high cost and difficult processing conditions.[3,4] To overcome these drawbacks numerous studies were carried out on conductive polymers which are promising alternatives to be used as a TE material.

Their abundance, low cost, wide range of applications, non-toxicity, good mechanical properties, good electrical conductivity, and low thermal conductivity make conductive polymers a potential for use as a TE material. The TE performances of the conductive polymers are mainly examined by the power factor (PF = $S^2\sigma$) due to their low intrinsic thermal conductivity.[5] Therefore, it is crucial to enhance the Seebeck coefficient and electrical conductivity in order to increase the TE performance of conductive polymers.[6]

Among its counterparts, polyaniline (PANI), with unique properties such as ease of synthesis, tunable doping/dedoping process, good electrical properties, good environmental stability, and non-toxicity, has a wide range of applications such as anticorrosive coatings, batteries, semiconductors, sensors, and capacitors.[7–9] PANI can be classified into three

(Received December 23, 2020; accepted March 2, 2021; published online March 25, 2021)

oxidation states: leucoemeraldine (fully reduced state), pernigraniline (fully oxidized state), and emeraldine (50% oxidized state).[10] The non-conducting emeraldine base form can be converted into the conductive emeraldine salt by doping with acids. The conductivity properties of emeraldine salt can be tuned with the dopant ratio.[11] The electrical conductivity of pristine PANI ranges from 10^{-7} S cm^{-1} to 300 S cm^{-1} depending on its oxidation states. With the doping process, the electrical conductivity of PANI can be enhanced 10-fold.[12] Nath et al. reported that the *ZT* of PANI reached 2.17 at 17 K by doping with camphorsulfonic acid (CSA).[13]

The incorporation of organic or inorganic fillers is another way to improve the TE properties of the conductive polymers. Recently, several studies have been conducted on the addition of carbon-based materials such as carbon nanotubes, graphite, and graphene to PANI.[14–21]. In these studies, it has been reported that the incorporation of carbon-based materials significantly enhanced the TE properties of PANI.

Graphitic carbon nitride (g-C_3N_4), a metal-free semiconductor, is generally used as photocatalyst, sensor, and photovoltaics due to its tunable optoelectronic properties, high surface area, selectivity, and chemical stability[22]. g-C_3N_4 can be easily obtained from various low-cost precursors, namely, cyanamide, urea, thiourea, guanidine-HCl, melamine and dicyandiamide via one-step polymerization[23]. g-C_3N_4 has a 2-dimensional structure composed of N-bridged tri-s-triazine repeating units.[24] The weak van der Waals forces between the layers lead to a honeycomb-like arrangement of atoms with strong covalent bonds, leading to the formation of g-C_3N_4 in a graphite-like structure.[25] Furthermore, the nitrogen-rich structure of g-C_3N_4 provides a strong electronegativity that leads to more advantages compared to graphene in electrochemistry and semiconductor applications[26]. In addition, Mortazavi et al. mentioned that the κ of g-C_3N_4 is around 7.6 W m^{-1} K^{-1} and 3.5 W m^{-1} K^{-1} which are two orders of magnitude lower compared to graphene sheets.[27] Despite its unique properties, there are few studies on the TE properties of g-C_3N_4. Shyni et al. reported that *ZT* of bismuth antimony telluride increased from 0.295 to 1.09 with the addition of the g-C_3N_4.[28] Ding et al. also reported that *ZT* of the layered carbon nitride reached up to 0.52 at 300 K.[29]

In this study, we investigated the TE properties of the nanocomposite films of PANI doped with CSA and g-C_3N_4 (PANI-CSA/g-C_3N_4) at different weight ratios in ambient conditions.

MATERIALS AND METHODS

Materials

Aniline (99%), guanidine hydrochloride (≥98%), camphor-10-sulfonic acid (98%), ammonium persulfate (98%), hydrochloric acid (37%), ammonia solution (25%), acetone (≥99.5%), and m-cresol (99%), were purchased from Merck, Germany, and used without a further purification.

Synthesis of g-C_3N_4

The synthesis of g-C_3N_4 was carried out as described in the literature.[30] Five grams of guanidine-HCl was put into a ceramic crucible and heated to 500°C for 4 h at a heating rate of 10°C min^{-1}. After the heating process, a yellowish powder was obtained. The obtained powder was dispersed in distilled water with the weight ratios of 1% and the dispersion was ultra-sonicated for 30 min to obtain nano-g-C_3N_4. The particle size of g-C_3N_4 was measured as 90 ± 3 nm.

Synthesis of PANI-CSA

Firstly, 3.92 mL (0.3 M) of aniline was dispersed in 80 mL of 1 M HCl solution. Then, 20 mL of 0.6 M ammonium persulfate solution was added dropwise into the monomer solution. The polymerization was carried out for 16 h at ambient conditions. The obtained dark green polymer was washed with distilled water and acetone to remove the impurities. Immediately after, the dedopping process was carried out by the dispersion of appropriate amount of PANI in 1 M ammonia solution for 24 h. After the dedopping process, the emeraldine base form of PANI was dissolved in m-cresol with a weight ratio of 0.5%. Finally, PANI-CSA solution was obtained by the addition of camphor-10-sulfonic acid (PANI:-dopant ratio of 1:2) to the solution. The doping process was carried out 24 h.

Preparation of PANI/ g-C_3N_4 Nanocomposites

PANI/g-C_3N_4 nanocomposites were prepared by ultrasonic homogenization to contain 1%, 5%, 10%, 20%, 30%, 40%, and 50% g-C_3N_4 by weight. Appropriate amounts of g-C_3N_4 nanoparticles were added into the solution of PANI-CSA in m-cresol with a weight ratio of 0.5%. The composite solutions were homogenized at a frequency of 20 kHz for 30 min. The composite films were cast on the glass substrates which were successively washed with piranha solution, distilled water, and acetone. Then, the composite films were dried in an oven under vacuum at 80°C for 12 h.

Characterization

The chemical nature of the samples were characterized by FTIR (Thermo Fisher Scientific Nicolet IS10) and UV-Vis (Shimadzu UVmini-1240) spectroscopy. The crystalline structure of the samples were obtained by using XRD with Cu Kα radiation (I= 1.54°Å) (T&T TT-90 X-ray diffractometer, operated at 30 mA and 40 KVP MAX) analysis. The morphological analyses were carried out using a scanning electron microscope (SEM) (Zeiss EVO® LS 10). Conductivities and Seebeck coefficient

measurements were carried out using a Four-Point Probe (Entek Electronic FPP 470) and Seebeck coefficient measuring device (Entek Electronic Seebeck Coefficient Measuring System).

RESULTS AND DISCUSSION

The XRD patterns of g-C_3N_4, PANI-CSA, and the composite with 40% g-C_3N_4 were shown in Fig.1. The graphite-like structure can be observed from the pattern of g-C_3N_4. The broad peak at 13.0° is related to in-planar repeating units while the sharp peak at 27.6° indicating to stacked layers.[31] For PANI-CSA, the sharp peaks at 14.9°, 20.9°, and 25.4° are the characteristics and indicate the crystalline structure of PANI-CSA.[32] Considering the pattern of the composite, peaks similar to PANI-CSA were observed. This similarity indicates that no additional crystal structure is included in the composite.[33] This can be attributed to the surface of the g-C_3N_4 particles homogeneously dispersed in the matrix, completely coated by the polymer[34].

SEM images of g-C_3N_4, PANI-CSA, and the composite with 40% g-C_3N_4 are illustrated in Fig. 2. The granular structure of PANI-CSA is due to the growth of polymer chains without entanglement during polymerization (Fig. 2b).[35] From the image of the composite, the graphite-like layers of g-C_3N_4 are clearly visible in the PANI-CSA matrix (Fig. 2c).

The FTIR-ATR spectra of g-C_3N_4, PANI-CSA, and the composite with 40% g-C_3N_4 are given in the Fig. 3. In the spectrum of g-C_3N_4, the peak at 3170 cm^{-1} corresponds to N–H stretching. The band observed at 1620 cm^{-1} and the peak at 1230 cm^{-1} belong to C=N and C–N stretchings, respectively. In addition, the C–N bending peak of the triazine units is obtained at around 800 cm^{-1}.[36,37] From the spectrum of PANI-CSA, the peaks at 1552 cm^{-1} and 1416 cm^{-1} are attributed to quinoid and benzenoid ring stretchings, respectively. Moreover, the peak at 1152 cm^{-1} is the characteristics of doped PANI which is the result of strong π–π interactions in the structure. The peaks of the sulfonic acid groups are at 1028 cm^{-1} and 793 cm^{-1}.[38,39]

For the composite, it was observed that the addition of g-C_3N_4 did not change the spectrum of PANI-CSA. This may be as a result of the homogeneous distribution of the nanoscale g-C_3N_4 particles in the matrix. However, it was observed that the peaks of the composite were slightly shifted to lower wavenumbers. This can be attributed to the addition of semiconducting g-C_3N_4 nanoparticles leading to increased electron conjugation of the PANI-CSA.

UV–Vis spectra of PANI-CSA and the composites are given in Fig. 4. During the analysis, the samples were prepared so as to have equal concentrations. The absorption bands observed around 430 nm are due to polaron–π^* transitions, whereas the broad band around 660 nm corresponds to the isolated

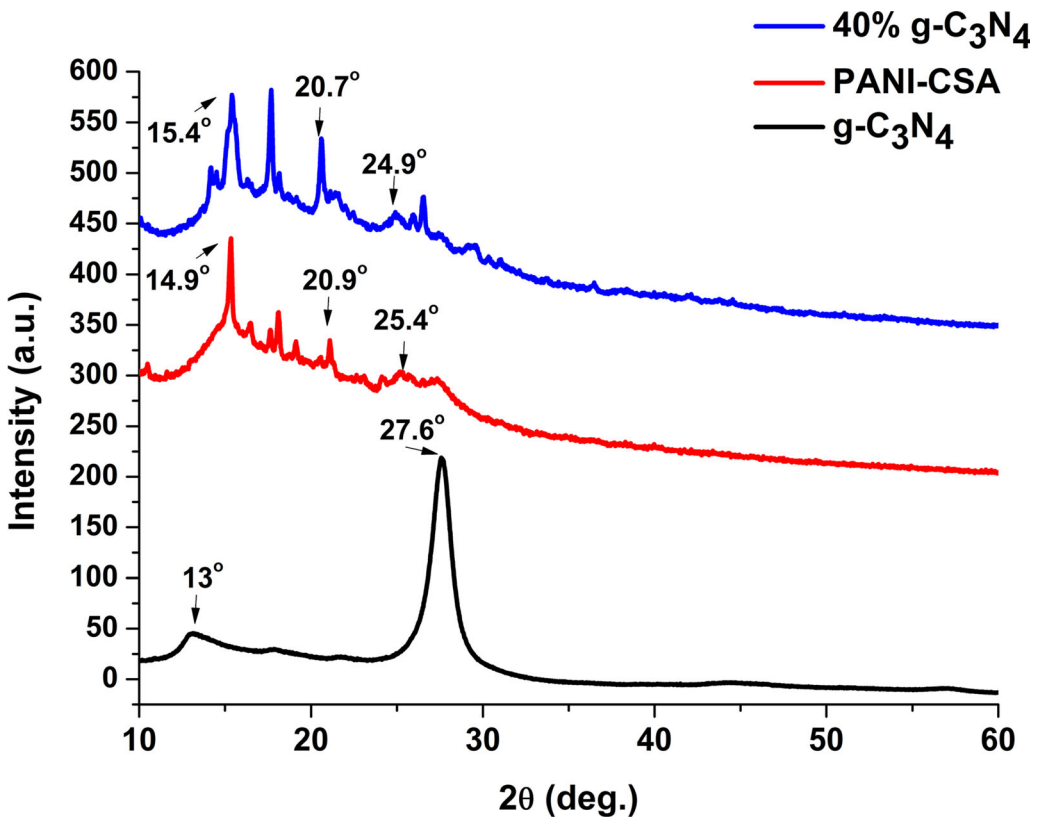

Fig 1. XRD patterns of g-C_3N_4, PANI-CSA, and the composite with 40% g-C_3N_4.

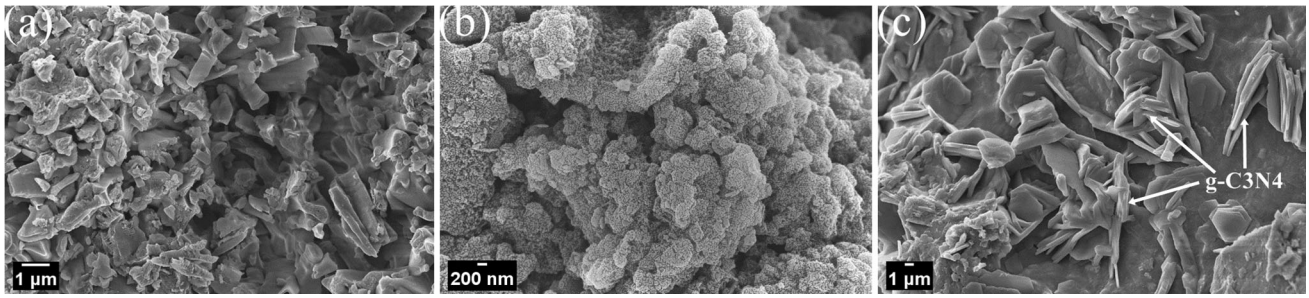

Fig 2. SEM images of the samples; g-C_3N_4 (a), PANI-CSA (b), and the composite with 40% g-C_3N_4 (c).

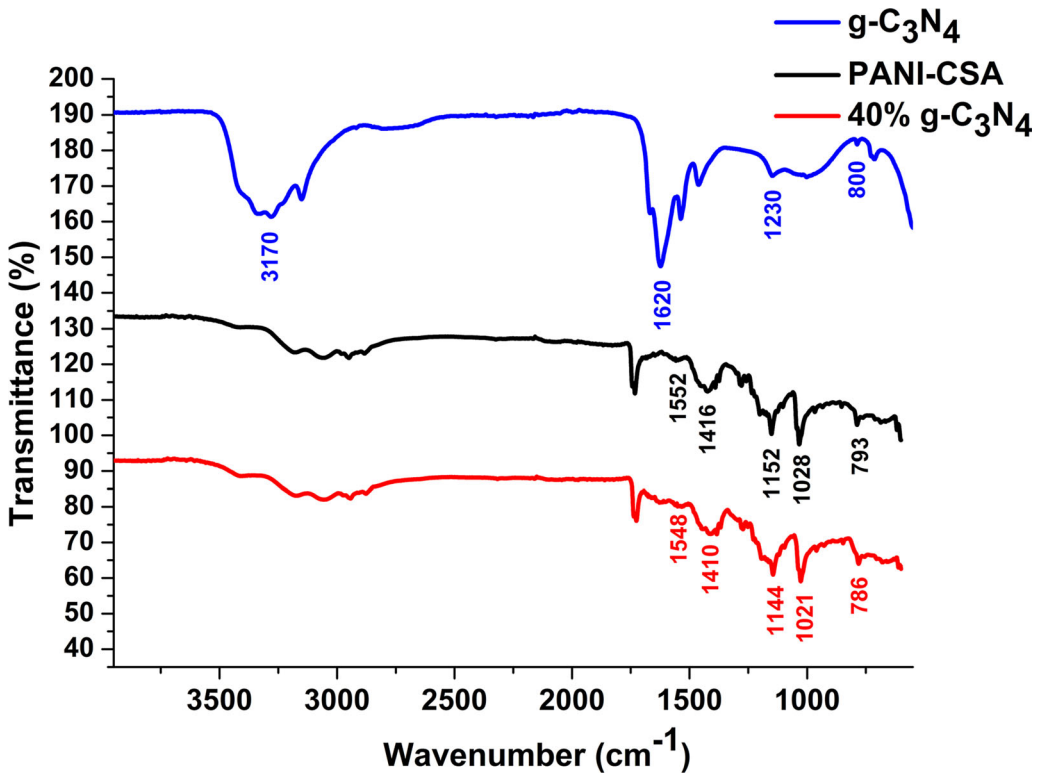

Fig 3. FTIR-ATR spectra of g-C_3N_4, PANI-CSA, and the composite with 40% g-C_3N_4.

polaron band transitions. The band around 830 nm can be assigned as π–polaron transitions of the charge carriers.[40] The delocalization of polarons can be resulted from the conformation of the PANI from a compact form to an expanded form by doping with CSA. Yao et al. stated that the dissolution of CSA doped PANI in m-cresol forms H-bonds between carbonyl groups in CSA structure and hydroxyl groups in m-cresol structure. This bond formation creates electrostatic repulsion between the positive charges in the polymer structure, causing the delocalization of polarons along the polymer chain.[41] It seems that electronegative groups of g-C_3N_4 negatively affect these interactions and reduces the delocalization of polarons.

Thermoelectric properties of g-C_3N_4, PANI-CSA, and the composites with different g-C_3N_4 weight ratios are given in Fig. 5. The conductivity measurements were carried out at room temperature while the Seebeck coefficients were measured at 293 K and 343 K at the cold and hot ends of the samples. The PF of the samples was calculated using the equation PF = σS^2.

The conductivity, Seebeeck coefficient, and PF of PANI-CSA are 15 S cm^{-1}, 10 μV K^{-1}, and 0.15 μW m^{-1} K^{-2}, respectively. The conductivity decreases steadily as g-C_3N_4 is added. The highest conductivity of the composites is measured as 14.7 S cm^{-1} for the composite with 1% g-C_3N_4. Considering the Seebeck coefficient measurements, it was observed that all the samples show a positive Seebeck coefficient which is a characteristics of *p-type* semiconductors. This indicates that the charge is carried by the holes, that is, positively signed bipolarons or polarons.[42,43] Among the composites, the largest Seebeck coefficient was obtained as 472 μV K^{-1} for the composite containing 50% g-C_3N_4. Generally speaking, due to the inverse correlation

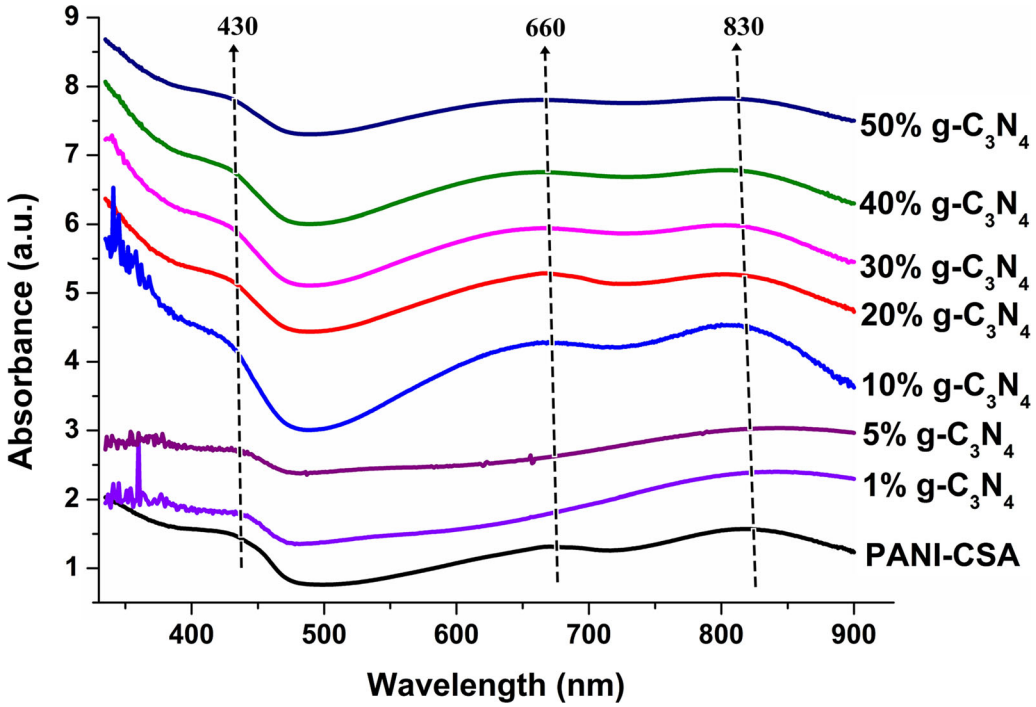

Fig 4. UV–Vis spectra of PANI-CSA and the composites with g-C_3N_4 ratios of 10%, 20%, 30%, 40%, and 50%.

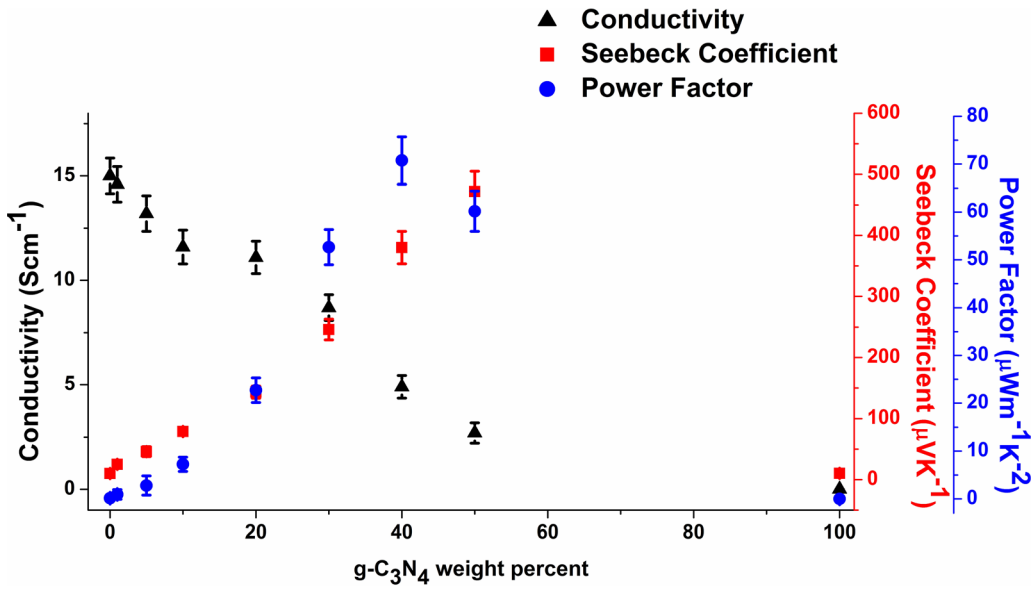

Fig 5. Conductivity, Seebeck coefficient and power factor of g-C_3N_4, PANI-CSA, and the composites.

between electrical conductivity and the Seebeck coefficient, they are expected to change in opposite directions with respect to each other.[44] All the composite samples are in agreement with this situation. The highest PF calculated from electrical conductivities and Seebeck coefficients was obtained as 70.75 μW m^{-1} K^{-2} in the sample containing 40% g-C_3N_4. Since there are no data on TE properties of PANI/GCN composites in the literature, the TE properties of the composites prepared in this study were compared with the data reported for PANI/carbon-based material composites and are given in Table I. Considering the data given in Table I, it can be seen that the composites synthesized in this study have considerably higher Seebeck coefficient values among their counterparts. The PF value of the composite containing 40% g-C_3N_4 is comparable with the highest one in the table.

Table I. The comparison of the TE properties of the composites prepared in this study and with literature data

Sample	Conductivity (S cm^{-1})	Seebeck coefficient ($\mu V\ K^{-1}$)	Power factor ($\mu W\ m^{-1}\ K^{-2}$)	References
PANI/g-C_3N_4 (40% g-C_3N_4)	4.9	380	70.75	This study
PANI/g-C_3N_4 (50% g-C_3N_4)	2.7	472	60.16	This study
PANI/graphene	856	~ 15	19	17
PANI/graphene	~ 400	~ 45	81.9	4
PANI/graphite	1.2×10^4	18.66	4.18	20
PANI/CNT	~ 61.47	28.6	5.0433	19
PANI/graphene	130	~ 15	3.6	45
PANI/graphene oxide	18.08	32.64	~ 2	46
PANI/graphene	3677	24	214	14
PANI/graphene	814	26	55	47
PANI/graphene	1300	33.34	14.6	48
PANI/graphene	58.89	31.0	5.6	49

CONCLUSION

In the present study, the TE performances of CSA doped PANI/g-C_3N_4 composites were investigated. Despite the decrease in electrical conductivity, with the addition of 50% g-C_3N_4, the Seebeck coefficient of the composite reached up to 472 $\mu V\ K^{-1}$ which is almost 50-fold larger than that of pristine PANI-CSA while with the addition of 40% g-C_3N_4, the PF reached up to 70.75 $\mu W\ m^{-1}\ K^{-2}$ which is about 500 times higher than that of pristine. Also, all composite samples showed positive Seebeck coefficient values specific to *p-type* semiconductors. This study suggests that a low-cost, abundant, non-toxic and sustainable g-C_3N_4 is a promising additive for producing polymer-based TE materials that can be used at room temperature.

ACKNOWLEDGMENTS

Financial support for this study has been provided by the Scientific and Technological Research Council of Turkey (TUBITAK) for supporting our study (Project No. 119M213).

CONFLICT OF INTEREST

We declare that they have no conflict of interest.

REFERENCES

1. N. Nandihalli, C.-J. Liu, and T. Mori, *Nano Energy* 78, 105186 (2020).
2. V. Ugraskan, and F. Karaman, *J. Electr. Mater.* 49, 7560 (2020).
3. K. Yusupov, D. Hedman, A.P. Tsapenko, A. Ishteev, S. You, V. Khovaylo, A. Larsson, A.G. Nasibulin, and A. Vomiero, *J. Alloys Compd.* 845, 156354 (2020).
4. Y.-Y. Hsieh, Y. Zhang, L. Zhang, Y. Fang, S.N. Kanakaraaj, J.-H. Bahk, and V. Shanov, *Nanoscale* 11, 6552 (2019).
5. S. Wang, F. Liu, C. Gao, T. Wan, L. Wang, L. Wang, and L. Wang, *Chem. Eng. J.* 370, 322 (2019).
6. S. Wang, Y. Zhou, Y. Liu, L. Wang, and C. Gao, *J. Mater. Chem. C* 8, 528 (2020).
7. A. Debnath, K. Deb, K. Sarkar, and B. Saha, *J. Electr. Mater.* 49, 5028 (2020).
8. F. Yakuphanoglu, B.F. Şenkal, and A. Sarac, *J. Electr. Mater.* 37, 930 (2008).
9. W. Yang, H. Xu, Y. Li, and W. Wang, *J. Electr. Mater.* 46, 4815 (2017).
10. J. De Albuquerque, L.H.C. Mattoso, R.M. Faria, J.G. Masters, and A.G. MacDiarmid, *Synth. Met.* 146, 1 (2004).
11. A. Zoshki, M.B. Rahmani, F. Masdarolomoor, and S.H. Pilehrood, *J. Nanoelectron. Optoelectron.* 12, 465 (2017).
12. M. Bharti, A. Singh, S. Samanta, and D.K. Aswal, *Prog. Mater. Sci.* 93, 270 (2018).
13. C. Nath, A. Kumar, Y.-K. Kuo, and G.S. Okram, *Appl. Phys. Lett.* 105, 133108 (2014).
14. T. Ube, J. Koyanagi, T. Kosaki, K. Fujimoto, T. Yokozeki, T. Ishiguro, and K. Nishio, *J. Mater. Sci.* 54, 3904 (2019).
15. T.N.A.B.T.A. Mutalib, S.J. Tan, K.L. Foo, Y.M. Liew, C.Y. Heah, and M.M.A.B. Abdullah, *Polym. Bull.* (2020). https://doi.org/10.1007/s00289-020-03334-w.
16. V. Shalini, M. Navaneethan, S. Harish, J. Archana, S. Ponnusamy, H. Ikeda, and Y. Hayakawa, *Appl. Surf. Sci.* 493, 1350 (2019).
17. L. Wang, Q. Yao, H. Bi, F. Huang, Q. Wang, and L. Chen, *J. Mater. Chem. A* 2, 11107 (2014).
18. R. Wu, H. Yuan, C. Liu, J.-L. Lan, X. Yang, and Y.-H. Lin, *RSC Adv.* 8, 26011 (2018).
19. C. Meng, C. Liu, and S. Fan, *Adv. Mater.* 22, 535 (2010).
20. L. Wang, D. Wang, G. Zhu, J. Li, and F. Pan, *Mater. Lett.* 65, 1086 (2011).
21. M. Culebras, C.M. Gómez, and A. Cantarero, *Materials* 7, 6701 (2014).
22. N. Rono, J.K. Kibet, B.S. Martincigh, and V.O. Nyamori, *Crit. Rev. Solid State Mater. Sci.* (2020). https://doi.org/10.1080/10408436.2019.1709414.
23. Z. Zhao, Y. Sun, and F.J.N. Dong, *Nanoscale* 7, 15 (2015).
24. H.-B. Fang, Y. Luo, Y.-Z. Zheng, W. Ma, and X. Tao, *Ind. Eng. Chem. Res.* 55, 4506 (2016).
25. A. Mishra, A. Mehta, S. Basu, N.P. Shetti, K.R. Reddy, and T.M. Aminabhavi, *Carbon* 149, 693 (2019).
26. Y. Ma, Y. Yang, C. Lu, K. Lu, S. Wu, X. Liu, and X. Wen, *J. Appl. Polym. Sci.* 135, 46242 (2018).
27. B. Mortazavi, G. Cuniberti, and T. Rabczuk, *Comput. Mater. Sci.* 99, 285 (2015).

28. P. Shyni, P.P. Pradyumnan, P. Rajasekar, A.M. Narayanan, and A.M. Umarji, *J. Alloys Compd.* 853, 156872 (2021).
29. Z. Ding, M. An, S. Mo, X. Yu, Z. Jin, Y. Liao, K. Esfarjani, J.-T. Lü, J. Shiomi, and N. Yang, *J. Mater. Chem. A* 7, 2114 (2019).
30. L. Shi, L. Liang, F. Wang, J. Ma, and J. Sun, *Catal. Sci. Technol.* 4, 3235 (2014).
31. J. Liu, T. Zhang, Z. Wang, G. Dawson, and W. Chen, *J. Mater. Chem.* 21, 14398 (2011).
32. B.S. Singu, P. Srinivasan, and S. Pabba, *J. Electrochem. Soc.* 159, A6 (2011).
33. Y. Duan, J. Liu, Y. Zhang, and T. Wang, *RSC Adv.* 6, 73915 (2016).
34. Y. Zhang, J. Liu, Y. Zhang, J. Liu, and Y. Duan, *RSC Adv.* 7, 54031 (2017).
35. H.S. Hassan, M.F. Elkady, M.A. Abd El kawi, and M. Alian, *Am. J. Appl. Chem.* 3, 54 (2015).
36. K. Ramesh, M. Prashantha, N.K. Reddy, and E.S.R. Gopal, *Integr. Ferroelectr.* 117, 40 (2010).
37. M. Kim, S. Hwang, and J.-S. Yu, *J. Mater. Chem.* 17, 1656 (2007).
38. S. Saravanan, C.J. Mathai, M.R. Anantharaman, S. Venkatachalam, and P.V. Prabhakaran, *J. Phys. Chem. Solids* 67, 1496 (2006).
39. R.R. Mohan, S.J. Varma, M. Faisal, and S. Jayalekshmi, *RSC Adv.* 5, 5917 (2015).
40. J.E. Osorio-Fuente, C. Gómez-Yáñez, M. de Ángeles-Hernández-Pérez, and F. Pérez-Moreno, *J. Mex. Chem. Soc.* 58, 52 (2014).
41. Q. Yao, Q. Wang, L. Wang, Y. Wang, J. Sun, H. Zeng, Z. Jin, X. Huang, and L. Chen, *J. Mater. Chem. A* 2, 2634 (2014).
42. K.J. Erickson, F. Léonard, V. Stavila, M.E. Foster, C.D. Spataru, R.E. Jones, B.M. Foley, P.E. Hopkins, M.D. Allendorf, and A.A. Talin, *Adv. Mater.* 27, 3453 (2015).
43. O. Abdulrazzaq, S.E. Bourdo, V. Saini, F. Watanabe, B. Barnes, A. Ghosh, and A.S. Biris, *RSC Adv.* 5, 33 (2015).
44. H. Yao, Z. Fan, H. Cheng, X. Guan, C. Wang, K. Sun, and J. Ouyang, *Macromol. Rapid Commun.* 39, 1700727 (2018).
45. Y. Harima, S. Fukumoto, L. Zhang, X. Jiang, J. Yano, K. Inumaru, and I. Imae, *RSC Adv.* 5, 86855 (2015).
46. M. Mitra, C. Kulsi, K. Chatterjee, K. Kargupta, S. Ganguly, D. Banerjee, and S. Goswami, *RSC Adv.* 5, 31039 (2015).
47. L. Wang, Q. Yao, H. Bi, F. Huang, Q. Wang, and L. Chen, *J. Mater. Chem. A* 3, 7086 (2015).
48. Y. Wang, J. Yang, L. Wang, K. Du, Q. Yin, and Q. Yin, *ACS Appl. Mater. Interfaces* 9, 20124 (2017).
49. Y. Du, S.Z. Shen, W. Yang, R. Donelson, K. Cai, and P.S. Casey, *Synth. Met.* 161, 2688 (2012).